# Geometric Approach to Strapdown Magnetometer Calibration in Sensor Frame

**J. F. VASCONCELOS,** Student Member, IEEE
Instituto Superior Técnico
Portugal

**G. ELKAIM,** Member, IEEE
University of California Santa Cruz

**C. SILVESTRE,** Member, IEEE
**P. OLIVEIRA,** Member, IEEE
**B. CARDEIRA**
Instituto Superior Técnico
Portugal

**In this work a new algorithm is derived for the onboard calibration of three-axis strapdown magnetometers. The proposed calibration method is written in the sensor frame, and compensates for the combined effect of all linear time-invariant distortions, namely soft iron, hard iron, sensor nonorthogonality, and bias, among others. A maximum likelihood estimator (MLE) is formulated to iteratively find the optimal calibration parameters that best fit to the onboard sensor readings, without requiring external attitude references. It is shown that the proposed calibration technique is equivalent to the estimation of a rotation, scaling and translation transformation, and that the sensor alignment matrix is given by the solution of the orthogonal Procrustes problem. Good initial conditions for the iterative algorithm are obtained by a suboptimal batch least squares computation. Simulation and experimental results with low-cost sensors data are presented and discussed, supporting the application of the algorithm to autonomous vehicles and other robotic platforms.**

Manuscript received May 28, 2008; revised August 3, 2009; released for publication March 19, 2010.

IEEE Log No. T-AES/47/2/940846.

Refereeing of this contribution was handled by Y. Oshman.

This work was partially supported by Fundação para a Ciência e a Tecnologia (ISR/IST) plurianual funding) through the POS_Conhecimento Program that includes FEDER funds and by the project MEDIRES from ADI and project PDCT/MAR/55609/2004-RUMOS of the FCT.

The work of J. F. Vasconcelos was supported by a Ph.D. Student Scholarship, SFRH/BD/18954/2004, from the Portuguese FCT POCTI programme.

Authors' current addresses: J. F. Vasconcelos, C. Silvestre, P. Oliveira, and B. Cardeira, Institute for Systems and Robotics, Instituto Superior Técnico, Av. Rovisco Pais, No. 1, Torre Norte, 8° andar, 1049-001, Lisbon, Portugal; G. Elkaim, Autonomous Systems Lab, Dept. of Computer Engineering, University of California Santa Cruz, 1156 High St., SOE3, Santa Cruz, CA 95064, E-mail: (elkaim@soe.ucsc.edu).



## I. INTRODUCTION

Magnetometers are a key aiding sensor for attitude estimation in low-cost high-performance navigation systems [1–4], with widespread application to autonomous air, ground, and ocean vehicles. These inexpensive, low power sensors allow for accurate attitude estimates by comparing the magnetic field vector observation in body frame coordinates with the vector representation in Earth frame coordinates, available from geomagnetic charts and software [5]. In conjunction with vector observations provided by other sensors such as star trackers or pendulums, the magnetometer triad yields complete 3-DOF (degrees of freedom) attitude estimation [3, 6].

The magnetic field reading distortions occur in the presence of ferromagnetic elements found in the vicinity of the sensor and due to devices mounted in the vehicle's structure. Other sources of disturbances are associated with technological limitations in sensor manufacturing and installation. A comprehensive description of the magnetic compass theory can be found in [7].

Magnetometer calibration is an old problem in ship navigation and many calibration techniques have been presented in the literature. The classic compass swinging calibration technique proposed in [8] is a heading calibration algorithm that computes scalar parameters using a least squares algorithm. The major shortcoming of this approach is the necessity of an external heading information [9], which is a strong requirement in many applications. A tutorial work using a similar but more sound mathematical derivation is found in [7]. This book addresses the fundamentals of magnetic compass theory and presents a methodology to calibrate the soft and hard iron parameters in heading and pitch, resorting only to the magnetic compass data. However, the calibration algorithm is derived by means of successive approximations and is formulated in a deterministic fashion that does not exploit the data of multiple compass readings.

In recent literature, advanced magnetometer calibration algorithms have been proposed to tackle distortions such as bias, hard iron, soft iron, and nonorthogonality directly in the sensor space, with no external attitude references and using optimality criteria. The batch least squares calibration algorithm derived in [10], [9] accounts for nonorthogonality, scaling, and bias errors. A nonlinear, two-step estimator provides the initial conditions using a nonlinear change of variables to cast the calibration in a pseudolinear least squares form. The obtained estimate of the calibration parameters is then iteratively processed by a linearized least squares batch algorithm.

The TWOSTEP batch method proposed in [11] is based on the observations of the differences between the actual and the measured unit vector,

denoted as scalar-checking. In the first step of the algorithm, the centering approximation derived in [12] produces a good initial guess of the calibration parameters, by rewriting the calibration problem in a linear least squares form. In a second step, a batch Gauss-Newton method is adopted to iteratively estimate the bias, scaling, and nonorthogonality parameters. In related work, [13] derives recursive algorithms for magnetometer calibration based on the centering approximation and on nonlinear Kalman filtering techniques.

Magnetic errors such as soft iron, hard iron, scaling, bias, and nonorthogonality are modeled separately in [10]. Although additional magnetic transformations can be modeled, it is known that some sensor errors are compensated by an equivalent effect, e.g. the hard iron and sensor biases are grouped together in [9]. Therefore, the calibration procedure should address the estimation of the joint effect of the sensor errors, as opposed to estimating each effect separately.

In this work, the magnetometer reading error model is discussed and cast in an error formulation which accounts for the combined effect of all linear time-invariant magnetic transformations. A rigorous geometric formulation simplifies the problem of compensating for the modeled and unmodeled magnetometer errors to that of the estimation of parameters lying on an ellipsoid manifold. A complete methodology to calibrate the magnetometer is detailed, and a maximum likelihood estimator (MLE) allows for the formulation of the calibration problem as the optimization of the sensor readings likelihood.

The sensor calibration problem is naturally formulated in the sensor frame. The calibration parameters are estimated using the magnetometer readings, and without resorting to external information or models about the magnetic field. In addition, a closed-form solution for the sensor alignment is also presented, based on the well-known solution to the orthogonal Procrustes problem [14].

The proposed calibration methodology is assessed both in simulation and using experimental data. Because the calibration parameters are influenced by the magnetic characteristics of the payload, the geomagnetic profile of the terrain, and diverse vehicle operating conditions, the online calibration of the magnetometers is analyzed. The calibration parameters are estimated for magnetometer data collected in ring shaped sets, corresponding to yaw and pitch maneuvers that are feasible for most land, air, and ocean vehicles. Simulation and experimental results show that the algorithm performs a computationally fast calibration with accurate parameter estimation. The accuracy of the estimates is validated by comparing the calibration results with those obtained by the snapshot method previously proposed in [15] and by the TWOSTEP calibration algorithm [11].

To the best of the authors' knowledge, this work is an original rigorous derivation of a calibration algorithm using a comprehensive model of the sensor readings in $\mathbb{R}^3$, that clarifies and exploits the geometric locus of the magnetometer readings, given by an ellipsoid manifold. Using this geometric insight, this paper presents an algorithm that consolidates the snapshot calibration method presented in [15], and improves on the experimental results obtained therein. Also, it is shown that the calibration and alignment procedures are distinct.

This paper is organized as follows. In Section II, a unified magnetometer error parametrization is derived and formulated. It is shown that the calibration parameters describe an ellipsoid surface and that the calibration and alignment problems are distinct. An MLE formulation is proposed to calculate the optimal generic calibration parameters and an algorithm to provide good initial conditions is presented. Also, a closed-form solution for the magnetometer alignment problem is obtained. Simulation and experimental results obtained with a low-cost magnetometer triad are presented and discussed in Section III. Finally, Section IV draws concluding remarks and comments on future work.

## II. MAGNETOMETER CALIBRATION AND ALIGNMENT

In this section, an equivalent parametrization of the magnetometer errors is derived. The main sources of magnetic distortion and bias are characterized, to yield a comprehensive structured model of the magnetometer readings. Using this detailed parametrization as a motivation, the magnetometer calibration problem is recast, without loss of generality, into a unified transformation parametrized by a rotation $\mathcal{R}$, a scaling $\mathbf{S}$, and an offset $\mathbf{b}$. Consequently, it is shown that for all linear transformations of the magnetic field, such as soft and hard iron, nonorthogonality, scaling factor, and sensor bias, the magnetometer readings will always lie on an ellipsoid manifold.

An MLE formulation is proposed to find the optimal calibration parameters which maximize the likelihood of the sensor readings. The proposed calibration algorithm is derived in the sensor frame and does not require any specific information about the magnetic field's magnitude and body frame coordinates. This fact allows for magnetometer calibration without external aiding references. Also, a closed-form optimal algorithm to align the magnetometer and body coordinate frames is obtained from the solution to the orthogonal Procrustes problem.

### A. Magnetometer Errors Characterization

The magnetometer readings are distorted by the presence of ferromagnetic elements in the vicinity

of the sensor, the interference between the magnetic field and the vehicle structure, local permanently magnetized materials, and by sensor technological limitations.

*Hard Iron/Soft Iron*: The hard iron bias, denoted as $\mathbf{b}_{\mathrm{HI}}$, is the combined result of the permanent magnets inherent to the vehicle's structure, as well as other elements installed in the vehicle, and it is constant in the vehicle's coordinate frame.

Soft iron effects are generated by the interaction of an external magnetic field with the ferromagnetic materials in the vicinity of the sensor. The resulting magnetic field depends on the magnitude and direction of the applied magnetic field with respect to the soft iron material, producing

$$\mathbf{h}_{\mathrm{SI}} = \mathbf{C}_{\mathrm{SI}} {}^{B}_{E}\mathbf{R}\, {}^{E}\mathbf{h} \tag{1}$$

where $\mathbf{C}_{\mathrm{SI}} \in \mathrm{M}(3)$ is the soft iron transformation matrix, ${}^{E}_{B}\mathbf{R}$ is the rotation matrix from body to Earth coordinate frames, ${}^{B}_{E}\mathbf{R} := {}^{E}_{B}\mathbf{R}'$, ${}^{E}\mathbf{h}$ is the Earth magnetic field, $\mathrm{M}(n,m)$ denotes the set of $n \times m$ matrices with real entries and $\mathrm{M}(n) := \mathrm{M}(n,n)$. As described in [7, ch. XI], the combined hard and soft iron effects are given by $\mathbf{h}_{\mathrm{SI}+HI} = \mathbf{h}_{\mathrm{SI}} + \mathbf{b}_{\mathrm{HI}}$. The linearization of the ferromagnetic effects (1) yields the well-known heading error $\delta\psi$ model [7, 9] adopted in compass swinging calibration, which ignores the harmonics above $2\psi$. The formulation (1), adopted in this paper, yields a rigorous approach to the simultaneous estimation of the hard and soft iron effects.

*Nonorthogonality*: The nonorthogonality of the sensors can be described as a transformation of vector space basis, parametrized by

$$\mathbf{C}_{\mathrm{NO}} = \begin{bmatrix} 1 & 0 & 0 \\ \sin(\rho) & \cos(\rho) & 0 \\ \sin(\phi)\cos(\lambda) & \sin(\lambda) & \cos(\phi)\cos(\lambda) \end{bmatrix}$$

where $(\rho, \phi, \lambda)$ are, respectively, the misalignment angles between the $y$-sensor and the $y$-axis, the $z$-sensor and the $x$-$z$ plane, and the $z$-sensor and the $y$-$z$ plane; more details on the adopted model of magnetometer misalignment errors can be found in [15].

*Scaling and Bias*: The null-shift or offset of the sensor readings is modeled as a constant vector $\mathbf{b}_M \in \mathbb{R}^3$. The transduction from the electrical output of the sensor to the measured quantity is formulated as a scaling matrix $\mathbf{S}_M \in \mathrm{D}^+(3)$, where $\mathrm{D}(n)$ denotes the set of $n \times n$ diagonal matrices with real entries and $\mathrm{D}^+(n) = \{\mathbf{S} \in \mathrm{D}(n) : \mathbf{S} > 0\}$.

*Wideband Noise*: The disturbing noise is assumed wideband compared with the bandwidth of the system, yielding uncorrelated sensor sampled noise.

*Alignment with the Body Frame*: The formulation of the proposed algorithm in the sensor frame allows for sensor calibration without determination of the alignment of the sensor with respect to a reference frame. An alignment procedure of the sensor triad is proposed in this paper for the sake of completeness.

*Other Effects*: Generic and more complex effects related to sensor-specific characteristics and to the magnetic distortion are difficult to model accurately. The proposed calibration algorithm compensates for the combined influence of all linear time-invariant transformations that distort the magnetic field, which are estimated in the form of an equivalent linear transformation.

### B. Magnetometer Error Parametrization

This section formulates an equivalent error model of the magnetometer measurements. First, the estimation problem of the nonideal magnetic effects described in Section IIA is recast, without loss of generality, as the problem of estimating an affine linear transformation. Second, it is shown that the linear transformation is equivalent to a single rotation, scaling, and translation transformation. In other words, to calibrate the magnetometer it is sufficient to estimate the center, orientation, and radii of the ellipsoid that best fit to the acquired data. Also, the derived sensor model is used to show that the magnetometer alignment cannot be determined using only sensor frame information, which implies that the calibration and the alignment problems must be addressed separately.

Define the unit sphere and an ellipsoid as [16]

$$\mathrm{S}(n) = \{\mathbf{x} \in \mathbb{R}^{n+1} : \|\mathbf{x}\|^2 = 1\}$$

$$\mathrm{L}(n) = \{\mathbf{x} \in \mathbb{R}^{n+1} : \|\mathbf{S}\mathcal{R}'\mathbf{x}\|^2 = 1\}$$

where $\mathbf{S} \in \mathrm{D}^+(n+1)$ and $\mathcal{R} \in \mathrm{SO}(n+1)$ describe the radii and orientation of the ellipsoid, respectively, and $\mathrm{SO}(n) = \{\mathcal{R} \in \mathrm{O}(n) : \det(\mathcal{R}) = 1\}$, $\mathrm{O}(n) = \{\mathbf{U} \in \mathrm{M}(n) : \mathbf{U}\mathbf{U}' = \mathbf{I}_n\}$. The three-axis magnetometer reading is given by the Earth's magnetic field ${}^{E}\mathbf{h}$ affected by the magnetic distortions and errors, yielding

$$\mathbf{h}_{ri} = \mathbf{S}_M \mathbf{C}_{\mathrm{NO}} (\mathbf{C}_{\mathrm{SI}} {}^{B}_{E}\mathbf{R}_i \|{}^{E}\mathbf{h}\| {}^{E}\bar{\mathbf{h}}_i + \mathbf{b}_{\mathrm{HI}}) + \mathbf{b}_M + \mathbf{n}_{mi} \tag{2}$$

where $\mathbf{h}_r$ is the magnetometer reading in the (nonorthogonal) magnetometer coordinate frame, ${}^{E}\bar{\mathbf{h}}_i = {}^{E}\mathbf{h}_i / \|{}^{E}\mathbf{h}\|$ is the unit vector obtained by normalizing ${}^{E}\mathbf{h}_i$, $\mathbf{n}_m \in \mathbb{R}^3$ is the Gaussian wideband noise, $\mathbf{S}_M$, $\mathbf{C}_{\mathrm{NO}}$, $\mathbf{C}_{\mathrm{SI}}$, $\mathbf{b}_{\mathrm{HI}}$, and $\mathbf{b}_M$ are the magnetic distortions described in Section IIA, and $i = 1, \ldots, n$ denotes the index of the reading. The model (2) assumes that $\|{}^{E}\mathbf{h}\|$ is constant, which allows for an intuitive geometric analysis of the magnetometer calibration problem. Nonetheless, the derived results are subsequently extended for the more general case where the magnitude is diverse for each $i$.

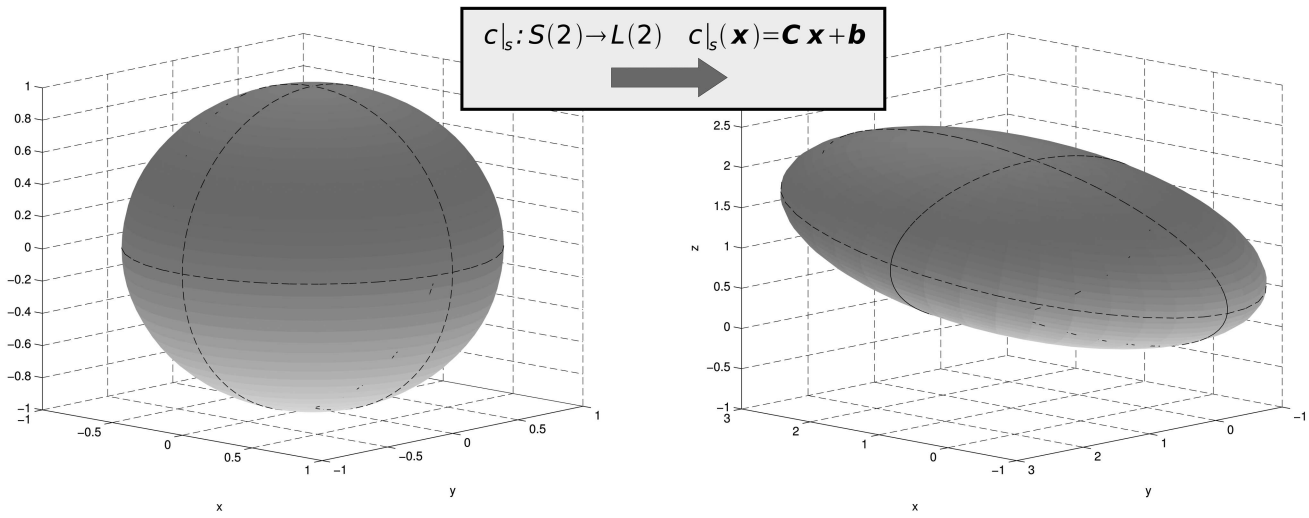


Fig. 1. Affine transformation of two-dimensional sphere.

Without loss of generality, the magnetometer reading can be described by

$$\mathbf{h}_{ri} = \mathbf{C}\,{}^{B}\bar{\mathbf{h}}_i + \mathbf{b} + \mathbf{n}_{mi} \tag{3}$$

where $\mathbf{C} = \mathbf{S}_M\mathbf{C}_{\text{NO}}\mathbf{C}_{\text{SI}}\|{}^{E}\mathbf{h}\|$, $\mathbf{b} = \mathbf{S}_M\mathbf{C}_{\text{NO}}\mathbf{b}_{\text{HI}} + \mathbf{b}_M$, ${}^{B}\bar{\mathbf{h}}_i = {}^{B}_{E}\mathbf{R}_i\,{}^{E}\bar{\mathbf{h}}_i$, ${}^{B}\bar{\mathbf{h}}_i \in \mathrm{S}(2)$ is the normalized magnetic field in body coordinate frame. In particular, $\mathbf{C} \in \mathrm{M}(3)$ and $\mathbf{b} \in \mathbb{R}^3$ are unconstrained, so unmodeled linear time-invariant magnetic errors and distortions are also taken into account. It is also clear that $\mathbf{S}_M$, $\mathbf{C}_{\text{NO}}$, $\mathbf{C}_{\text{SI}}$, $\mathbf{b}_{\text{HI}}$, and $\mathbf{b}_M$ are unobservable because diverse solutions for these parameters can be computed given $\mathbf{C}$ and $\mathbf{b}$.

Given that the points ${}^{B}\bar{\mathbf{h}}_i$ are contained in the sphere, straightforward application of the singular value decomposition (SVD) [16] shows that the magnetometer readings $\mathbf{h}_{ri}$ lie on an ellipsoid manifold, as illustrated in the example of Fig. 1 and summarized in the following theorem. The proof is presented for the sake of clarity.

THEOREM 1 ([16]) *Let $c : \mathbb{R}^n \to \mathbb{R}^n$, $c(\mathbf{x}) = \mathbf{C}\mathbf{x}$ be a linear transformation where $\mathbf{C} \in \mathrm{M}(n)$ is full rank. Then $c(\mathbf{x})$ is a bijective transformation between the sphere and an ellipsoid in $\mathbb{R}^n$, i.e., there is an ellipsoid $\mathrm{L}(n-1)$ such that the transformation $c|_{\mathrm{S}} : \mathrm{S}(n-1) \to \mathrm{L}(n-1)$, $c|_{\mathrm{S}}(\mathbf{x}) = \mathbf{C}\mathbf{x}$ is bijective.*

PROOF Denote the SVD of $\mathbf{C}$ as $\mathbf{C} = \mathbf{U}\Sigma\mathbf{V}'$, where $\mathbf{U}, \mathbf{V} \in \mathrm{O}(n)$, and $\Sigma \in \mathrm{D}^+(n)$. Define the matrices $\mathcal{R}_L := \mathbf{U}\mathbf{J}$, $\mathbf{S}_L := \Sigma$, $\mathbf{V}_L := \mathbf{V}\mathbf{J}$,

$$\mathbf{J} := \begin{bmatrix} \det(\mathbf{U}) & \mathbf{0} \\ \mathbf{0} & \mathbf{I}_{n-1} \end{bmatrix},$$

which describe a modified SVD with at least one special orthogonal matrix $\mathbf{C} = \mathcal{R}_L\mathbf{S}_L\mathbf{V}_L'$ where $\mathcal{R}_L \in \mathrm{SO}(n)$, $\mathbf{S}_L \in \mathrm{D}^+(n)$, and $\mathbf{V}_L \in \mathrm{O}(n)$. The transformation $c(\mathbf{x})$ applied to the sphere is given by

$$c|_{\mathrm{S}}(\mathbf{x}) := \mathcal{R}_L\mathbf{S}_L\mathbf{y} \tag{4}$$

where $\mathbf{y} := \mathbf{V}_L'\mathbf{x}$ verifies $\|\mathbf{y}\|^2 = 1$. Choosing the ellipsoid $\mathrm{L}(n-1) = \{\mathbf{x} \in \mathbb{R}^n : \|\mathbf{S}_L^{-1}\mathcal{R}_L'\mathbf{x}\|^2 = 1\}$ then $c|_{\mathrm{S}}(\mathbf{x}) \in \mathrm{L}(n-1)$. The function (4) is injective because $\mathcal{R}_L\mathbf{S}_L$ is invertible. To see that it is surjective, given any $\mathbf{z} \in \mathrm{L}(n-1)$, the point $\mathbf{y} = \mathbf{S}_L^{-1}\mathcal{R}_L'\mathbf{z} \in \mathrm{S}(n-1)$ satisfies $c(\mathbf{y}) = \mathbf{z}$.

COROLLARY 1 *Let $\mathbf{C} \in \mathrm{M}(n)$ be a full rank matrix and let the SVD of $\mathbf{C}$ be given by $\mathbf{C} = \mathcal{R}_L\mathbf{S}_L\mathbf{V}_L'$ where $\mathcal{R}_L \in \mathrm{SO}(n)$, $\mathbf{S}_L \in \mathrm{D}^+(n)$ and $\mathbf{V}_L \in \mathrm{O}(n)$. The ellipsoid described by $c|_{\mathrm{S}}$ is spanned by the bijective transformation $l : \mathrm{S}(n-1) \to \mathrm{L}(n-1)$, $l(\mathbf{x}) = \mathcal{R}_L\mathbf{S}_L\mathbf{x}$.*

Theorem 1 implies that the magnetic field readings $\mathbf{h}_{ri}$ derived in (3) lie on the surface of an ellipsoid centered on $\mathbf{b}$, referred to as sensor ellipsoid. Corollary 1 states that the sensor ellipsoid centered at $\mathbf{b}$ is fully characterized the rotation $\mathcal{R}_L$ and scaling $\mathbf{S}_L$ matrices. Consequently, the calibration process is equivalent to the estimation of the ellipsoid's parameters $\mathbf{b}$, $\mathcal{R}_L$, and $\mathbf{S}_L$.

Motivated by these results, and denoting the SVD of $\mathbf{C}$ as $\mathbf{C} = \mathcal{R}_L\mathbf{S}_L\mathbf{V}_L'$, the equivalent model for the magnetometer readings (3) can be described by

$$\mathbf{h}_{ri} = \mathcal{R}_L\mathbf{S}_L\,{}^{C}\bar{\mathbf{h}}_i + \mathbf{b} + \mathbf{n}_{mi} \tag{5}$$

where ${}^{C}\bar{\mathbf{h}}_i := \mathbf{V}_L'\,{}^{B}\bar{\mathbf{h}}_i$, ${}^{C}\bar{\mathbf{h}}_i \in \mathrm{S}(2)$, and the matrix $\mathbf{V}_L \in \mathrm{O}(3)$ is a fixed orthogonal transformation between $\{B\}$ and the sensor frame $\{C\}$, and is referred to as alignment matrix. Although alignment matrices are commonly associated with SO(3), the slight relaxation in the definition of alignment matrix is adopted for sake of generality, so that $\mathbf{V}_L$ can model sensor setups where rotation and reflection may occur. Nonetheless, the case where it is possible to guarantee that $\mathbf{V}_L \in \mathrm{SO}(3)$ is also considered in the discussion of the alignment process.

The sensor model (5) evidences that ${}^{C}\bar{\mathbf{h}}_i$ can be computed given the calibration parameters ($\mathcal{R}_L$, $\mathbf{S}_L$, $\mathbf{b}$).

However the alignment matrix $\mathbf{V}_L$, which transforms ${}^C\bar{\mathbf{h}}_i$ to ${}^B\bar{\mathbf{h}}_i$, cannot be determined in the calibration process because ${}^B\bar{\mathbf{h}}_i$ is not measured. Consequently, the calibration and alignment problems are distinct.

The sensor calibration and alignment algorithm is structured as follows. In the calibration step, the parameters $\mathcal{R}_L$, $\mathbf{S}_L$, and $\mathbf{b}$ are estimated, using an MLE formulated on $\mathrm{M}(3)\times\mathbb{R}^3$. In the alignment step, the determination of the orthogonal transformation $\mathbf{V}_L$ is obtained from a closed-form optimal algorithm using vector readings in $\{C\}$ and $\{B\}$ frames.

### C. Maximum Likelihood Estimation of an Ellipsoid

In this work, the calibration parameters expressed in (5) are computed using an MLE. This section formulates the estimation of the ellipsoid parameters ($\mathcal{R}_L$, $\mathbf{S}_L$, $\mathbf{b}$) as an optimization problem on the manifold $\Theta := \mathrm{SO}(3)\times\mathrm{D}^+(3)\times\mathbb{R}^3$. Although optimization tools on Riemannian manifolds are required to solve for the calibration parameters directly on $\Theta$, see [17], [18] for a comprehensive introduction to the subject, an equivalent calibration can be performed on the Euclidean space $\mathrm{M}(3)\times\mathbb{R}^3$. The intermediate derivation of the MLE on the manifold $\Theta$, presented in this section, provides geometric insight on the cost functional, and evidences the assumptions underlying the derivation of MLE.

Assuming that the noise on the magnetometer readings is a zero mean Gaussian process with variance $\sigma_{mi}^2$, the probability density function (pdf) of each $\mathbf{h}_{ri}$ is also Gaussian

$$\mathbf{n}_{mi}\sim\mathcal{N}(0,\sigma_{mi}^2\mathbf{I})\Rightarrow\mathbf{h}_{ri}\sim\mathcal{N}(\mathcal{R}_L\mathbf{S}_L{}^C\bar{\mathbf{h}}_i+\mathbf{b},\sigma_{mi}^2\mathbf{I}).$$

The MLE finds the parameters that maximize the conditional pdf of each sensor reading given the optimization parameters [19]. The resulting minimization problem of the weighted log-likelihood function is described by

$$\min_{\substack{(\mathcal{R}_L,\mathbf{S}_L,\mathbf{b})\in\Theta\\ {}^C\bar{\mathbf{h}}_i\in\mathrm{S}(2),i=1,\dots,n}}\sum_{i=1}^{n}\left(\frac{\|(\mathbf{h}_{ri}-\mathbf{b})-\mathcal{R}_L\mathbf{S}_L{}^C\bar{\mathbf{h}}_i\|}{\sigma_{mi}}\right)^2. \tag{6}$$

The minimum of (6) is computed iteratively by gradient or Newton-like methods on manifolds [17, 18]. Note that solving the minimization problem (6) implies estimating $n$ auxiliary magnetic field vectors ${}^C\bar{\mathbf{h}}_i$, and the dimension of the search space is $(2n+\dim\Theta)$ whereas the dimension of the calibration parameters space is $\dim\Theta=\dim\mathrm{SO}(3)+\dim\mathrm{D}^+(3)+\dim\mathbb{R}^3=9$.

The minimization problem (6) finds the ellipsoid points $(\mathcal{R}_L\mathbf{S}_L{}^C\bar{\mathbf{h}}_i)$ that best fit the sensor readings $(\mathbf{h}_{ri}-\mathbf{b})$. Intuitively, the minimization problem can be rewritten to find the sphere points ${}^C\bar{\mathbf{h}}_i$ that best fit to the pullback of the ellipsoid to the sphere $(\mathbf{S}_L^{-1}\mathcal{R}_L'(\mathbf{h}_{ri}-\mathbf{b}))$, yielding

$$\min_{\substack{(\mathcal{R}_L,\mathbf{S}_L,\mathbf{b})\in\Theta\\ {}^C\bar{\mathbf{h}}_i\in\mathrm{S}(2),i=1,\dots,n}}\sum_{i=1}^{n}\left(\frac{\|\mathbf{S}_L^{-1}\mathcal{R}_L'(\mathbf{h}_{ri}-\mathbf{b})-{}^C\bar{\mathbf{h}}_i\|}{\sigma_{mi}}\right)^2. \tag{7}$$

The minimization problem (7) is suboptimal with respect to the unified error model (5), but can be rigorously derived using an MLE formulation by assuming that the main sources of electromagnetic noise are external to the sensor, that is

$$\begin{aligned}\mathbf{h}_{ri}&=\mathbf{S}_M\mathbf{C}_{\mathrm{NO}}(\mathbf{C}_{\mathrm{SI}}({}^B_E\mathbf{R}_i\|{}^E\mathbf{h}\|{}^E\bar{\mathbf{h}}+{}^B_N\mathbf{R}\mathbf{n}_{mi})+\mathbf{b}_{\mathrm{HI}})+\mathbf{b}_M\\&=\mathbf{C}{}^B\bar{\mathbf{h}}_i+\mathbf{C}{}^B_N\mathbf{R}\mathbf{n}_{mi}+\mathbf{b}\\&=\mathcal{R}_L\mathbf{S}_L{}^C\bar{\mathbf{h}}_i+\mathcal{R}_L\mathbf{S}_L\mathbf{V}'_{LN}{}^B_N\mathbf{R}\mathbf{n}_{mi}+\mathbf{b}\end{aligned} \tag{8}$$

where ${}^B_N\mathbf{R}$ rotates from the coordinate frame $\{N\}$ where the magnetic noise is defined, to the body coordinate frame. Assuming that $\mathbf{n}_{mi}$ is a zero mean Gaussian process with variance $\sigma_{mi}^2$, the pdf of each $\mathbf{h}_{ri}$ is also Gaussian

$$\mathbf{n}_{mi}\sim\mathcal{N}(0,\sigma_{mi}^2\mathbf{I})\Rightarrow\mathbf{h}_{ri}\sim\mathcal{N}(\mathcal{R}_L\mathbf{S}_L{}^C\bar{\mathbf{h}}_i+\mathbf{b},\sigma_{mi}^2\mathcal{R}_L\mathbf{S}_L^2\mathcal{R}_L').$$

Using the pdf of the $\mathbf{h}_{ri}$, straightforward analytical derivations show that MLE formulation is given by (7).

As convincingly argued in [20], if the noise exists in the sensor frame (5), the ellipsoid obtained by (7) tends to fit best the points with lower eccentricity. This effect can be balanced by defining appropriate curvature weights [20] $\sigma_{mi}^2$, producing results close to the optimal solution of (6). More important, the log-likelihood function (7) can be optimized by searching only in the parameter space $\Theta$.

PROPOSITION 1 *The solution* $(\mathcal{R}_L^*,\mathbf{S}_L^*,\mathbf{b}^*)$ *of* (7) *also minimizes*

$$\min_{(\mathcal{R}_L,\mathbf{S}_L,\mathbf{b})\in\Theta}\sum_{i=1}^{n}\left(\frac{\|\mathbf{S}_L^{-1}\mathcal{R}_L'(\mathbf{h}_{ri}-\mathbf{b})\|-1}{\sigma_{mi}}\right)^2. \tag{9}$$

PROOF Given $(\mathcal{R}_L^*,\mathbf{S}_L^*,\mathbf{b}^*)$, the optimal ${}^C\bar{\mathbf{h}}_i^*$ satisfies

$${}^C\bar{\mathbf{h}}_i^*=\arg\min_{{}^C\bar{\mathbf{h}}_i\in\mathrm{S}(2)}\|\mathbf{v}_i^*-{}^C\bar{\mathbf{h}}_i\|^2 \tag{10}$$

where $\mathbf{v}_i^*:=\mathbf{S}_L^{*-1}\mathcal{R}_L^{*\prime}(\mathbf{h}_{ri}-\mathbf{b}^*)$. The minimization problem (10) corresponds to the projection of $\mathbf{v}_i^*$ on the unit sphere, which has the closed-form solution ${}^C\bar{\mathbf{h}}_i^*=\mathbf{v}_i^*/\|\mathbf{v}_i^*\|$. Therefore, the minimization problem (7) can be written as

$$\min_{(\mathcal{R}_L,\mathbf{S}_L,\mathbf{b})\in\Theta}\sum_{i=1}^{n}\left(\frac{\left\|\mathbf{S}_L^{-1}\mathcal{R}_L'(\mathbf{h}_{ri}-\mathbf{b})-\dfrac{\mathbf{v}_i}{\|\mathbf{v}_i\|}\right\|}{\sigma_{mi}}\right)^2$$

where $\mathbf{v}_i:=\mathbf{S}_L^{-1}\mathcal{R}_L{}'(\mathbf{h}_{ri}-\mathbf{b})$. Using simple algebraic manipulation produces the likelihood function (9).

### D. Magnetometer Calibration Algorithm

In this section, the MLE presented on Proposition 1 is recast as a optimization problem on an Euclidean space, which allows for the use of optimization tools for unconstrained problems [21]. In the next proposition, the MLE is formulated on $\mathrm{M}(3)\times\mathbb{R}^3$.

PROPOSITION 2 *Let* $(\mathbf{T}^*,\mathbf{b}_T^*)$ *denote the solution of the unconstrained minimization problem*

$$\min_{\mathbf{T}\in\mathrm{M}(3),\mathbf{b}_T\in\mathbb{R}^3}\sum_{i=1}^{n}\left(\frac{\|\mathbf{T}(\mathbf{h}_{ri}-\mathbf{b}_T)\|-1}{\sigma_{mi}}\right)^2 \tag{11}$$

*and take the SVD of* $\mathbf{T}^*$*, given by* $\mathbf{T}^*=\mathbf{U}_T^*\mathbf{S}_T^*\mathbf{V}_T^{*\prime}$*, where* $\mathbf{U}_T\in\mathrm{O}(3)$*,* $\mathbf{S}_T\in\mathbf{D}^+(3)$*,* $\mathbf{V}_T\in\mathrm{SO}(3)$*. The solution of* (9) *is given by* $\mathcal{R}_L^*=\mathbf{V}_T^*$*,* $\mathbf{S}_L^*=\mathbf{S}_T^{*-1}$*,* $\mathbf{b}^*=\mathbf{b}_T^*$*.*

PROOF Using the equality $\|\mathbf{V}_L\mathbf{S}_L^{-1}\mathcal{R}_L'(\mathbf{h}_{ri}-\mathbf{b})\|=\|\mathbf{S}_L^{-1}\mathcal{R}_L'(\mathbf{h}_{ri}-\mathbf{b})\|$ for any $\mathbf{V}_L\in\mathrm{O}(3)$, and the fact that, by the SVD, $\mathbf{T}:=\mathbf{V}_L\mathbf{S}_L^{-1}\mathcal{R}_L'$ is a generic element of M(3), produces the desired results.

By Proposition 2, the parameters of the sensor model (5) are obtained by solving (11) and decomposing the resulting $\mathbf{T}^*$. Although (11) could be derived using (3) and the results of Section IIC expressed on $\mathrm{M}(3)\times\mathbb{R}^3$, the intermediate derivations (7) and (9) were formulated on $\Theta$ to show that 1) the sensor readings lie on an ellipsoid manifold parametrized by $\mathcal{R}_L$, $\mathbf{S}_L$, and $\mathbf{b}$, 2) the alignment matrix, represented by $\mathbf{V}_L$ (or $\mathbf{U}_T^*$) cannot be determined in the calibration process, given that there are no body referenced measurements, and 3) the optimization problem (7) can be solved by searching only in the space of the calibration parameters, using the formulation (9) derived for the sensor model given by (8).

A good initial guess of the calibration parameters is produced by the least squares estimator proposed in [15]. The locus of measurements described by

$$\|^E\mathbf{h}\|^2=\|\mathbf{C}^{-1}(\mathbf{h}_r-\mathbf{b})\|^2$$

is expanded and, by defining a nonlinear change of variables, it is rewritten as pseudolinear least squares estimation problem

$$H(\mathbf{h}_r)f(\mathbf{b},\mathbf{s})=b(\mathbf{h}_r) \tag{12}$$

where the matrix $H(\mathbf{h}_r)\in\mathrm{M}(n,9)$ and the vector $b(\mathbf{h}_r)\in\mathbb{R}^n$ are nonlinear functions of the vector readings and the vector of unknowns, $f(\mathbf{b},\mathbf{s})\in\mathbb{R}^6$ is a nonlinear function of the calibration parameters. The closed-form solution to the least squares problem (12) is found to yield a good first guess of the calibration parameters [15].

The calibration algorithm proposed in this work is summarized in the following. In the formulation of the calibration method, the $k$th estimate of the calibration parameters $(\mathbf{T},\mathbf{b})$ is denoted as $(\mathbf{T}_k,\mathbf{b}_k)$, and is concatenated in the vector $\mathbf{x}_k=[\mathrm{vec}'(\mathbf{T}_k)\ \ \mathbf{b}_k']'\in\mathbb{R}^{12}$, where vec is the column stacking operator [22]. The log-likelihood function defined in (11) is denoted by $f(\mathbf{x}):=\sum_{i=1}^{n}((\|\mathbf{T}(\mathbf{h}_{ri}-\mathbf{b})\|-1)/\sigma_{mi})^2$.

*Step 1 (Least Squares Estimator [15])* Compute the solution $\mathbf{p}$ to the least squares problem

$$\begin{bmatrix} h_{r1x}^2 & h_{r1x}h_{r1y} & h_{r1x}h_{r1z} & h_{r1y}^2 & h_{r1y}h_{r1z} & h_{r1x} & h_{r1y} & h_{r1z} & 1\\ \vdots & \vdots & \vdots & \vdots & \vdots & \vdots & \vdots & \vdots & \vdots\\ h_{rnx}^2 & h_{rnx}h_{rny} & h_{rnx}h_{rnz} & h_{rny}^2 & h_{rny}h_{rnz} & h_{rnx} & h_{rny} & h_{rnz} & 1 \end{bmatrix}\mathbf{p}=\begin{bmatrix} h_{r1z}^2\\ \vdots\\ h_{rnz}^2 \end{bmatrix} \tag{13}$$

where $\mathbf{p}\in\mathbb{R}^9$, and $h_{rix}$, $h_{riy}$, and $h_{riz}$ denote the $x$, $y$, and $z$ components of $\mathbf{h}_{ri}$, respectively. The initial estimates of the calibration parameters, $\mathbf{T}_0$ and $\mathbf{b}_0$, are given by

$$\mathbf{T}_0=\begin{bmatrix} \frac{1}{a} & 0 & 0\\ -\frac{1}{a}\tan\rho & -\frac{1}{b}\sec(\rho) & 0\\ \frac{1}{a}(\tan\rho\tan\lambda\sec\phi-\tan\phi) & -\frac{1}{b}\sec(\rho)\tan(\lambda)\sec(\phi) & \frac{1}{c}\sec(\lambda)\sec(\phi) \end{bmatrix},\qquad \mathbf{b}_0=\frac{1}{2\alpha_1}\begin{bmatrix}\beta_1\\ \beta_2\\ \beta_3\end{bmatrix}$$

where the parameters $(a,b,c)$, $(\rho,\theta,\phi)$ and $(\beta_1,\beta_2,\beta_3)$ are functions of $\mathbf{p}$, and can be obtained using equations (18) and (19) presented in the Appendix.

*Step 2 (Maximum Likelihood Estimator)* Set $k=0$. Compute

$$\begin{bmatrix}\mathrm{vec}(\mathbf{T}_{k+1})\\ \mathbf{b}_{k+1}\end{bmatrix}=\begin{bmatrix}\mathrm{vec}(\mathbf{T}_k)\\ \mathbf{b}_k\end{bmatrix}-(\nabla^2 f|_{\mathbf{x}_k})^{-1}\nabla f|_{\mathbf{x}_k} \tag{14}$$

using the algebraic formulation of the gradient and Hessian matrices (20) and (21), presented in the Appendix. Increment $k$ and repeat (14) until a stop

condition is satisfied, e.g. $\|\nabla f|_{\mathbf{x}_k}\| < \varepsilon_{\text{stop}}$ for a desired $\varepsilon_{\text{stop}}$.

*Step 3* The calibration parameters of the magnetometer model (3) are given by $\mathbf{C} = \mathbf{T}_k^{-1}$, $\mathbf{b} = \mathbf{b}_k$. The ellipsoid parameters $\mathcal{R}_L$ and $\mathbf{S}_L$ are given by the SVD $\mathbf{C} = \mathcal{R}_L \mathbf{S}_L \mathbf{V}_L'$.

Given the calibration parameters $(\mathcal{R}_L, \mathbf{S}_L, \mathbf{b})$, the representation of the Earth magnetic field in the calibration frame $\{C\}$ is obtained by algebraic manipulation of (5), resulting in

$$^C\mathbf{h}_i = \|^E\mathbf{h}\| \mathbf{S}_L^{-1} \mathcal{R}_L' (\mathbf{h}_{ri} - \mathbf{b}) \tag{15}$$

where the fact that $^C\mathbf{h}_i = \|^E\mathbf{h}\| {}^C\bar{\mathbf{h}}_i$ was used.

In the proposed calibration algorithm, the cost functional (11) is minimized using Newton's descent method [21], which yields very fast convergence near the minimum. The explicit formulations of $\nabla^2 f|_{\mathbf{x}_k}$ and $\nabla f|_{\mathbf{x}_k}$, presented in the Appendix, allow for the implementation of the Newton method without numerically approximating the Hessian and gradient matrices. For properties and variations of this method, the reader is referred to [21] and references therein.

As an alternative to the adopted least squares estimator, the algorithm proposed in [23] can produce an initial ellipsoid guess based on the difference-of-squares error criterion using a semidefinite programming (SDP) formulation. However, the SDP algorithm is computationally feasible only for no more than a few hundred samples, whereas the least squares estimator (13) allows for efficient processing of the several thousands of points contained in the calibration data, which are required in practice.

Note that the calibrated measurement (15) is obtained assuming that the magnitude of the Earth's magnetic field $\|^E\mathbf{h}\|$ is constant for the collected set of magnetometer measurements (2). This allows for an optimization problem (11) and a computation of $^C\bar{\mathbf{h}}_i$ that are independent of $\|^E\mathbf{h}\|$. In case $\|^E\mathbf{h}\|$ is known to fluctuate, namely due to collecting measurements at different geographic locations, the measurement model (3) can be written as

$$\frac{\mathbf{h}_{ri}}{\|^E\mathbf{h}_i\|} = \mathbf{C}\,{}^B\bar{\mathbf{h}}_i + \frac{\mathbf{b}}{\|^E\mathbf{h}_i\|} + \frac{\mathbf{n}_{mi}}{\|^E\mathbf{h}_i\|}$$

where $\mathbf{C}$ is now defined as $\mathbf{C} = \mathbf{S}_M \mathbf{C}_{\text{NO}} \mathbf{C}_{\text{SI}}$. Applying this measurement model directly in the result of Proposition 2, the log-likelihood function expressed in (11) is given by

$$\sum_{i=1}^{n} \frac{1}{\sigma_{mi}^2 \|^E\mathbf{h}_i\|^{-2}} \left( \left\| \mathbf{T} \left( \frac{\mathbf{h}_{ri}}{\|^E\mathbf{h}_i\|} - \frac{\mathbf{b}_T}{\|^E\mathbf{h}_i\|} \right) \right\| - 1 \right)^2$$

producing the optimization problem

$$\min_{\mathbf{T}\in \mathrm{M}(3), \mathbf{b}_T \in \mathbb{R}^3} \sum_{i=1}^{n} \left( \frac{\|\mathbf{T}(\mathbf{h}_{ri} - \mathbf{b}_T)\| - \|^E\mathbf{h}_i\|}{\sigma_{mi}^2} \right)^2$$

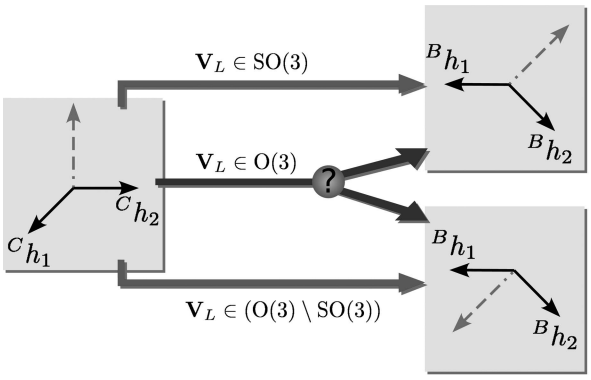


Fig. 2. Alignment estimation ambiguity with two vector readings.

where $\|^E\mathbf{h}_i\|$ is available from geomagnetic charts [5], and the weights $\sigma_{mi}$ can be inflated to compensate for modeling errors in $\|^E\mathbf{h}_i\|$. Given the solution $(\mathbf{T}, \mathbf{b}_T)$ of the modified maximum likelihood problem, the calibrated measurements are given by $^C\mathbf{h}_i = \mathbf{S}_L^{-1} \mathcal{R}_L' (\mathbf{h}_{ri} - \mathbf{b})$.

### E. Magnetometer Alignment

The representation of $^B\mathbf{h}_i$ in the body frame is necessary in attitude determination algorithms [6]. Although the alignment and calibration procedures are independent, the magnetometer alignment algorithm is detailed for the sake of completeness.

The magnetometer alignment with respect to a reference frame is represented by the orthogonal matrix $\mathbf{V}_L \in \mathrm{O}(3)$ contained in the unified transformation $\mathbf{C}$; see Corollary 1. Given that $^C\mathbf{h}_i := \mathbf{V}_L' {}^B\mathbf{h}_i, {}^C\mathbf{h}_i \in \mathrm{S}(2)$, the matrix $\mathbf{V}_L$ is computed using the $^C\mathbf{h}_i$ observations given by the calibrated sensor reading (15), and the $^B\mathbf{h}_i$ measurements obtained from external information sources, such as heading reference units or external localization systems.

As illustrated in Fig. 2, two vector readings are sufficient to characterize a rigid rotation $\mathbf{V}_L \in \mathrm{SO}(3)$, or a rotation with reflection $\mathbf{V}_L \in (\mathrm{O}(3) \setminus \mathrm{SO}(3))$, but the determination of an orthogonal transformation $\mathbf{V}_L \in \mathrm{O}(3)$ requires at least three linearly independent vectors readings. The well-known results for the orthogonal Procrustes problem [14] are adopted to determine $\mathbf{V}_L \in \mathrm{O}(3)$.

THEOREM 2 (Orthogonal Procrustes Problem) *Take two sets of vector readings in $\{C\}$ and $\{B\}$ coordinate frames, concatenated in the form $^C\mathbf{X} = [{}^C\mathbf{h}_1 \cdots {}^C\mathbf{h}_n]$ and $^B\mathbf{X} = [{}^B\mathbf{h}_1 \cdots {}^B\mathbf{h}_n]$ where $n \geq 3$. Assume that $^B\mathbf{X}\,{}^C\mathbf{X}'$ is nonsingular, and denote the corresponding SVD as $^B\mathbf{X}\,{}^C\mathbf{X}' = \mathbf{U}\Sigma\mathbf{V}'$, where $\mathbf{U}, \mathbf{V} \in \mathrm{O}(3)$, $\Sigma \in \mathrm{D}^+(3)$. The optimal orthogonal matrix $\mathbf{V}_L^* \in \mathrm{O}(3)$ that minimizes the transformation from $\{B\}$ to $\{C\}$ coordinates frames in the least squares sense*

$$\min_{\mathbf{V}_L \in \mathrm{O}(3)} \sum_{i=1}^{n} \|^C\mathbf{h}_i - \mathbf{V}_L' {}^B\mathbf{h}_i\|^2 \tag{16}$$

*is unique and given by $\mathbf{V}_L'^* = \mathbf{V}\mathbf{U}'$.*

TABLE I
Calibration Results (Gradient Method)

| | $f(\mathbf{x}_{-1})$ | $f(\mathbf{x}_0)$ | $f(\mathbf{x}^*)$ | Iterations | $\theta_e$ [rad] | $\mathbf{s}_e$ | $\mathbf{b}_e$ [G] |
|---|---|---|---|---|---|---|---|
| Ring shaped data | $3.28\times10^{-1}$ | $1.17\times10^{-4}$ | $9.64\times10^{-5}$ | 2246 | $1.74\times10^{-3}$ | $7.61\times10^{-3}$ | $3.54\times10^{-4}$ |
| Arch shaped data | $4.36\times10^{-1}$ | $1.18\times10^{-4}$ | $9.62\times10^{-5}$ | 1932 | $1.46\times10^{-2}$ | $1.65\times10^{-2}$ | $1.74\times10^{-2}$ |

TABLE II
Calibration Results (Newton Method)

| | $f(\mathbf{x}_{-1})$ | $f(\mathbf{x}_0)$ | $f(\mathbf{x}^*)$ | Iterations | $\theta_e$ [rad] | $\mathbf{s}_e$ | $\mathbf{b}_e$ [G] |
|---|---|---|---|---|---|---|---|
| Ring shaped data | $3.28\times10^{-1}$ | $1.18\times10^{-4}$ | $9.64\times10^{-5}$ | 37.0 | $1.74\times10^{-3}$ | $7.61\times10^{-3}$ | $3.54\times10^{-4}$ |
| Arch shaped data | $4.37\times10^{-1}$ | $1.18\times10^{-4}$ | $9.62\times10^{-5}$ | 37.2 | $1.46\times10^{-2}$ | $1.65\times10^{-2}$ | $1.75\times10^{-2}$ |

In applications where it can be guaranteed that $\mathbf{V}_L$ is a rotation matrix, i.e., $\mathbf{V}\in \mathrm{SO}(3)$, the solution to the Procrustes problem (16) is also the solution to the standard Wahba's problem [24], given by

$$\mathbf{V}_L'^{*} = \mathbf{V}\begin{bmatrix}1 & 0 & 0\\ 0 & 1 & 0\\ 0 & 0 & \det(\mathbf{V})\det(\mathbf{U})\end{bmatrix}\mathbf{U}'.$$

Using (15), the calibrated and aligned magnetic field vector reading is given by

$${}^{B}\mathbf{h}_i = \mathbf{V}_L{}^{C}\mathbf{h}_i$$

where ${}^{C}\mathbf{h}_i$ is the calibrated sensor measurement.

## III. ALGORITHM IMPLEMENTATION AND RESULTS

In this section, the proposed calibration algorithm is validated using simulated and experimental data from a triad of low-cost magnetometers.

### A. Simulation Results

The calibration algorithm was first analyzed using simulated data. The reference calibration parameters from (2) are

$$\mathbf{S}_M = \mathrm{diag}(1.2, 0.8, 1.3)$$

$$\begin{bmatrix}\psi\\ \theta\\ \phi\end{bmatrix} = \begin{bmatrix}2.0\dfrac{\pi}{180}\\ 1.0\dfrac{\pi}{180}\\ 1.5\dfrac{\pi}{180}\end{bmatrix}\ \mathrm{rad}$$

$$\mathbf{b}_{\mathrm{HI}} = \begin{bmatrix}-1.2\\ 0.2\\ -0.8\end{bmatrix}\mathrm{G}$$

$$\mathbf{b}_M = \begin{bmatrix}1.5\\ 0.4\\ 2.7\end{bmatrix}\mathrm{G}$$

$$\mathbf{C}_{\mathrm{SI}} = \begin{bmatrix}0.58 & -0.73 & 0.36\\ 1.32 & 0.46 & -0.12\\ -0.26 & 0.44 & 0.53\end{bmatrix}$$

and the magnetometer noise, described in the sensor space, is a zero mean Gaussian noise with standard deviation $\sigma_m = 5$ mG. The likelihood function $f$ is normalized by the number of samples $n$ and the stop condition of the minimization algorithm is $\|\nabla f|_{\mathbf{x}_k}\| < \varepsilon_{\mathrm{stop}} = 10^{-3}$. To benchmark the convergence rate and the optimization results of the Newton iterations (14), a gradient descent method is also studied. In this algorithm, the iterations are given by $\mathbf{x}_{k+1} = \mathbf{x}_k - \alpha_k \nabla f|_{\mathbf{x}_k}$, and the stepsize $\alpha_k$ is determined using the Armijo rule [21].

In a strapdown sensor architecture, the swinging of the magnetometer triad is constrained by the vehicle's maneuverability and, consequently, only some sections of the ellipsoid can be traced. The magnetic field readings are obtained for two specific cases, illustrated in Fig. 3. In the first case, a ring shaped uniform set of points is obtained for unconstrained yaw and a pitch sweep interval of $\theta\in[-20,20]^\circ$. Note that the constraint in the pitch angle can be found in most terrestrial vehicles. In the second case, the ellipsoid's curvature information is reduced by constraining the yaw to $\psi\in[-90,90]^\circ$.

The results of 20 Monte Carlo simulations using $10^4$ magnetometer readings are presented in Tables I and II and depicted in Fig. 3. Given the large likelihood cost of the noncalibrated data, denoted by $f(\mathbf{x}_{-1})$, the initial condition draws the cost function into the vicinity of the optimum, and the iterations yield a 20% improvement over the initial guess.

The Newton algorithm converges faster than the gradient algorithm, exploiting the second-order information of the Hessian, as illustrated in Fig. 4 and Fig. 5. Although the Hessian computations are more complex, the Newton method takes only 5 s to converge in a Matlab 7.3 implementation running on a standard computer with a Pentium Celeron 1.6 Ghz processor.

Defining the distance between the estimated and the actual parameter as $\mathbf{s}_e := \|\mathbf{S}^* - \mathbf{S}\|$, $\mathbf{b}_e := \|\mathbf{b}^* - \mathbf{b}\|$, and $\theta_e := \arccos((\mathrm{tr}(\mathcal{R}^*\mathcal{R}') - 1)/2)$, Tables I and II show that the arch shaped data set contains sufficient

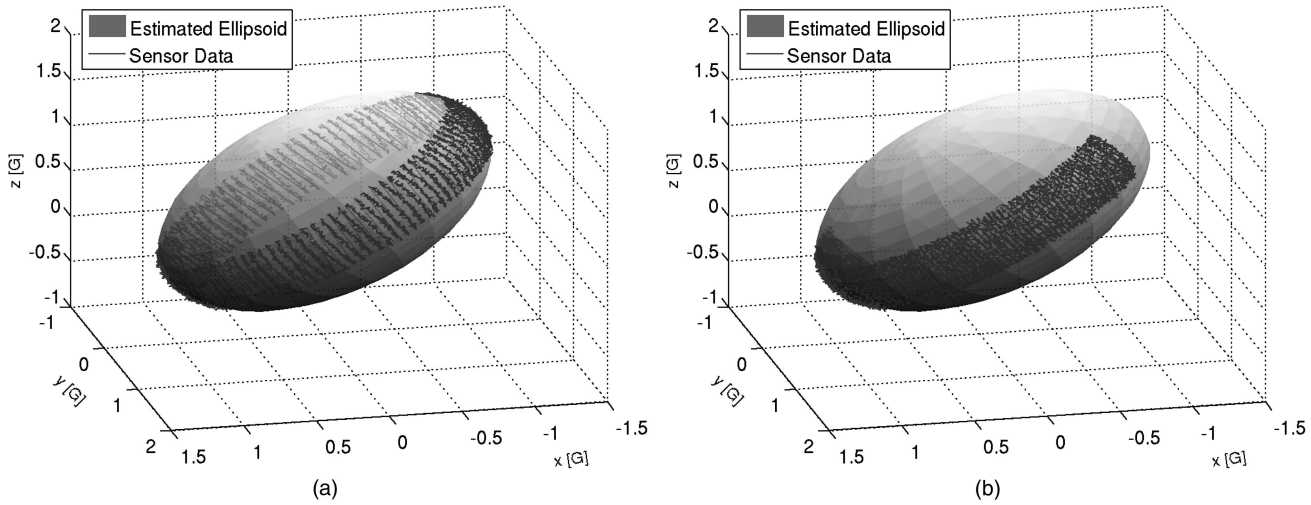


Fig. 3. Ellipsoid fitting (simulation data). (a) Ring-shaped data. (b) Arch-shaped data.

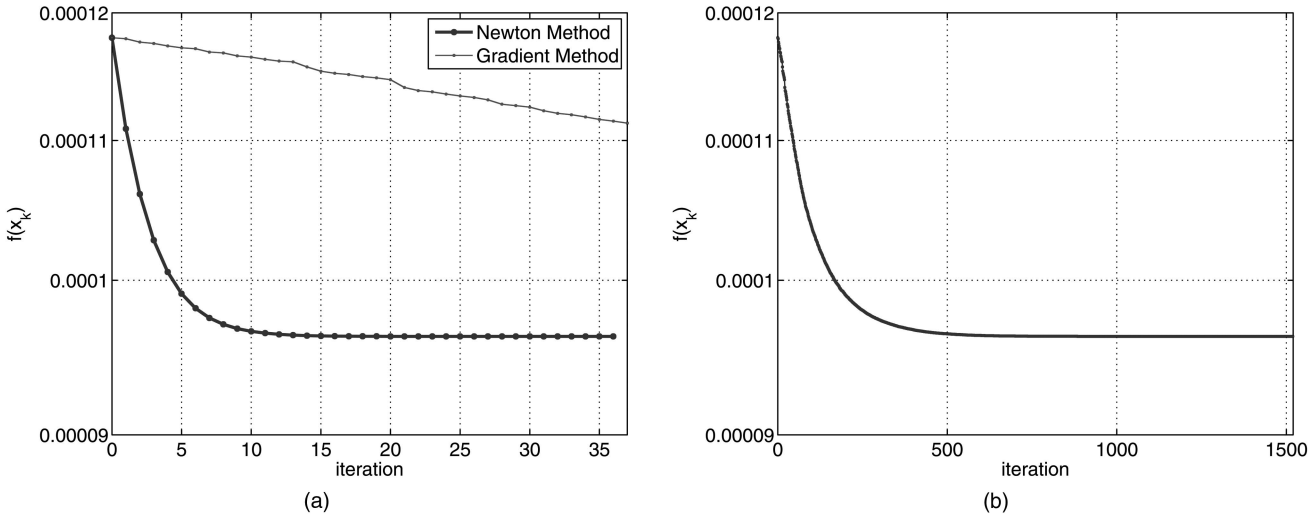


Fig. 4. Convergence of log-likelihood function (arch shaped data). (a) Newton (versus gradient) method. (b) Gradient method iterations.

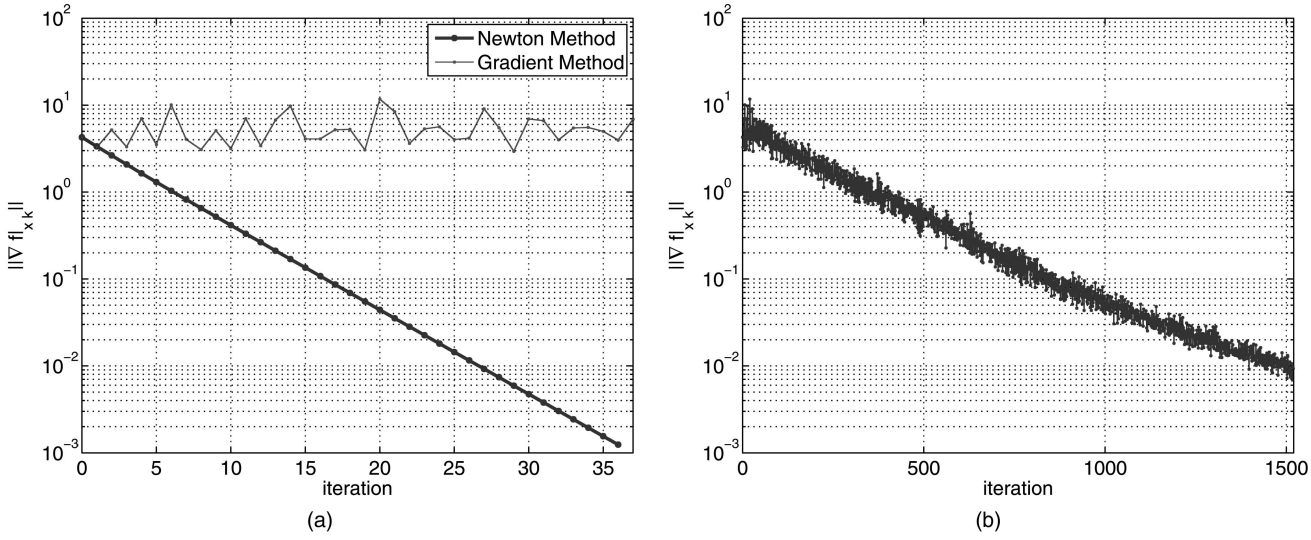


Fig. 5. Convergence of log-likelihood gradient (arch shaped data). (a) Newton (versus gradient) method. (b) Gradient method iterations.

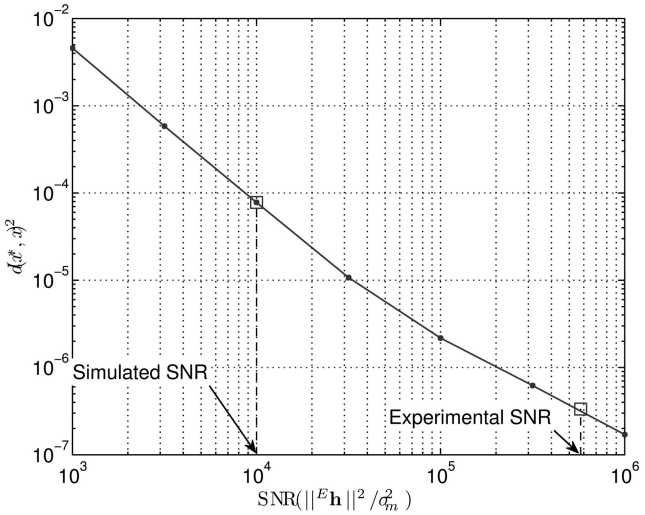


Fig. 6. Estimation error versus signal-to-noise ratio (100 MC, ring shaped data).

eccentricity information to estimate the equivalent magnetometer errors quantities $\mathcal{R}$, $\mathbf{s}$, and $\mathbf{b}$. Although the noise is formulated in the sensor frame, the suboptimal formulation (9) yields accurate results with uniform likelihood weights $\sigma_{mi}^2$, as depicted in Fig. 3. For platforms with limited maneuverability, the proposed optimization algorithm identifies the calibration parameters with good accuracy. As expected, reducing the information about the ellipsoid curvature slightly degrades the sensor calibration errors.

To validate the quality of the estimated parameters, an implementation of the TWOSTEP algorithm [11] was used to process the magnetometer measurements, yielding $(\theta_e, \mathbf{s}_e, \mathbf{b}_e) = (2.23 \times 10^{-3}$ rad, $5.08 \times 10^{-3}$, $4.41 \times 10^{-4}$ G) and $(\theta_e, \mathbf{s}_e, \mathbf{b}_e) = (1.12 \times 10^{-2}$ rad, $1.65 \times 10^{-2}, 1.42 \times 10^{-2}$ G) for the ring and arch shaped data, respectively. The results presented in Table II are similar to those obtained with the TWOSTEP algorithm, which validates the accuracy of the proposed calibration algorithm. These results also suggest that the magnetometer calibration methodologies presented in [11], [13], [15], and in this work can contribute to other fields of research where ellipsoid estimation is of interest, such as computer graphics, vision, statistics, pattern recognition, among others, for a representative list see [20], [23] and references therein.

The influence of the noise power in the estimation error is illustrated in Fig. 6, where the magnetic field magnitude in the San Francisco Bay area is adopted, $||^E\mathbf{h}|| = 0.5$ G, and the distance in the parameter space is given by $d(\mathbf{x}^*, \mathbf{x})^2 := \theta_e^2 + \mathbf{s}_e^2 + \mathbf{b}_e^2$.

## B. Experimental Results

The algorithm proposed in this work was used to estimate the calibration parameters for a set of $6 \times 10^4$ points obtained from an actual magnetometer triad. The magnetometer was a Honeywell HMC1042L 2-axis magnetometer and a Honeywell HMC1041Z for the third (Z) axis, sampled with a TI MSC12xx microcontroller with a 24 bit Delta Sigma converter, at 100 Hz; see [10] for details.

A gimbal system was maneuvered to collect 1) a set of sensor readings spanning the ellipsoid surface, Fig. 7(a), and 2) only four ellipsoid sections, Fig. 7(b). The calibration algorithm converged to a minimum within 60 Newton method iterations, taking less than 40 s and yielding $f(\mathbf{x}^*) = 2.51 \times 10^{-6}$ for the ellipsoid surface data set and $f(\mathbf{x}^*) = 2.67 \times 10^{-6}$ for the ellipsoid sections data set. Although the second data set included less data points, the results were similar because the collected data were sufficient to characterize the ellipsoid's eccentricity and rotation, as depicted in Fig. 7(b).

Given the calibration parameters, the sensor noise is characterized by rewriting (5) as $\mathbf{n}_{mi} = \mathbf{h}_r - (\mathcal{R}_L^* \mathbf{S}_L^* {}^C\bar{\mathbf{h}}_i^* + \mathbf{b}^*)$ where ${}^C\bar{\mathbf{h}}_i^*$ is given in the proof of Proposition 1. The obtained experimental standard

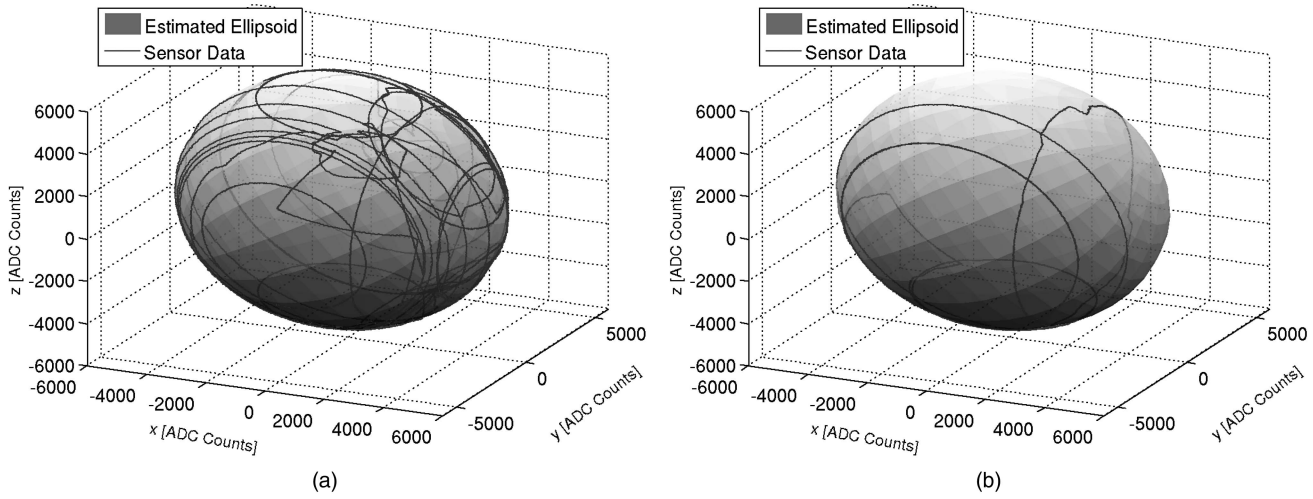


Fig. 7. Ellipsoid fitting (real data). (a) Ellipsoid surface data. (b) Ellipsoid sections data.

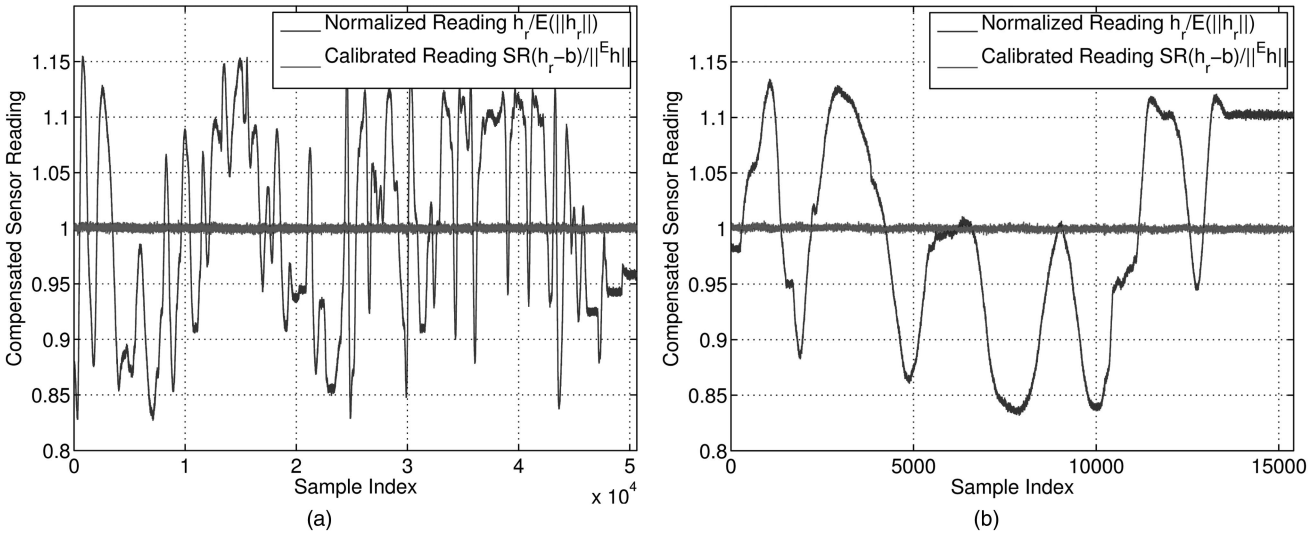


Fig. 8. Magnetometer data fitting. (a) Ellipsoid surface data. (b) Ellipsoid sections data.

deviation of the sensor noise is $\sigma_m = 0.65$ mG, which evidences that the signal-to-noise ratio of a typical low-cost magnetometer is better than that assumed in the simulations of Section IIIA, as depicted in Fig. 6.

The calibrated magnetometer data are compared with the raw data in Fig. 8. The calibrated readings are near to the unit circle locus, which validates the proposed unified error formulation of Theorem 1 and shows that the combined effect of the magnetic distortions is successfully compensated for.

## IV. CONCLUSIONS

A new estimation algorithm was derived and successfully validated for the onboard calibration of three-axis strapdown magnetometers. After a detailed characterization on the disturbances corrupting the magnetometer readings, an equivalent error parametrization was derived. The magnetometer calibration was shown to be equivalent to the estimation of an ellipsoid manifold. The parameter optimization problem was formulated resorting to an MLE, and an optimization algorithm was derived using the gradient and Newton descent methods. A closed-form solution for the magnetometer alignment was obtained from the solution to the orthogonal Procrustes problem. The performance of the proposed methodology was assessed both in simulation and with experimental data from low-cost sensors. Results show that the proposed calibration algorithm can be adopted for a wide variety of autonomous vehicles with maneuverability constraints and in situations that require periodic onboard sensor calibration.

Given the equivalence between magnetometer calibration and ellipsoid estimation evidenced in Section II, the algorithms proposed in [11], [13], [15], and in this work may provide new contributions to other research areas such as computer graphics, vision, statistics, and pattern recognition, where ellipsoid estimation is of paramount importance [23, 20]. Future work will exploit this circle of ideas, and the adaptation of the proposed algorithm to the 2D (heading only) case, for marine and land applications.

## APPENDIX. AUXILIARY RESULTS

This section presents auxiliary results adopted in the computations of the proposed calibration algorithm.

### A. Least Squares Estimation of the Calibration Parameters

The initialization of the calibration algorithm presented in Section IID is based on the magnetometer calibration algorithm proposed in [15]. The initial guess of the calibration parameters is obtained by solving the least squares estimation problem expressed in (13), and applying a nonlinear transformation to the solution $\mathbf{p}$ that yields the calibration parameters $(\mathbf{C}, \mathbf{b})$. In this section, the nonlinear transformation from $\mathbf{p}$ to $(\mathbf{C}, \mathbf{b})$ is detailed. Denote the components of the solution of the least squares problem as $\mathbf{p} = [A\ B\ C\ D\ E\ G\ H\ I\ J]'$, the calibration matrix and bias vector are given by

$$\mathbf{C} = \frac{1}{\|^E\mathbf{h}\|} \begin{bmatrix} a & 0 & 0 \\ b\sin(\rho) & b\cos(\rho) & 0 \\ c\sin(\phi)\cos(\lambda) & c\sin(\lambda) & c\cos(\phi)\cos(\lambda) \end{bmatrix} \tag{17}$$

$$\mathbf{b} = \frac{1}{2\alpha_1} \begin{bmatrix} \beta_1 \\ \beta_2 \\ \beta_3 \end{bmatrix}$$

where the scaling and the misalignment parameters are described by

$$\begin{aligned} a &= \frac{1}{2\alpha_1}(-(4D+E^2)\alpha_2)^{1/2} \\ b &= \frac{1}{2\alpha_1}(-(4A+C^2)\alpha_2)^{1/2} \\ c &= \frac{1}{2\alpha_1}((4DA-B^2)\alpha_2)^{1/2} \\ \tan\rho &= -\tfrac{1}{2}(2B+EC)(\alpha_1)^{-1/2} \\ \tan\phi &= (BE-2CD)(\alpha_1)^{-1/2} \\ \tan\lambda &= E(-\alpha_1\alpha_3^{-1})^{1/2} \end{aligned} \tag{18}$$

and the auxiliary variables are defined as

$$\begin{aligned} \beta_1 &= 2BH + BEI - 2CDI - 4DG + ECH - E^2G \\ \beta_2 &= -2AEI + 4AH - BCI - 2BG + C^2H - CEG \\ \beta_3 &= 4DIA - 2DGC + EGB - IB^2 - 2EHA + CBH \\ \alpha_1 &= -B^2 + DC^2 + 4DA + AE^2 - BEC \\ \alpha_2 &= 4AE^2J - E^2G^2 - 4BECJ + 2ECHG \\ &\quad + 2BEIG - 4EHAI - 4DICG - C^2H^2 \\ &\quad + 4DAI^2 + 2CBHI - 4DG^2 + 4DC^2J \\ &\quad + 4BHG - 4AH^2 - B^2I^2 - 4B^2J + 16DAJ \\ \alpha_3 &= E^4A - CBE^3 + E^2C^2D - 2B^2E^2 \\ &\quad + 8DAE^2 - 4DB^2 + 16D^2A. \end{aligned} \tag{19}$$

## B. Likelihood Function Derivatives

The calibration algorithm proposed in Section IID enhances the estimates given by (17), using optimization tools to solve a maximum likelihood estimation problem. This section presents the algebraic expressions for the gradient and Hessian of the likelihood function (11), used in descent optimization methods. Let $\mathbf{u}_i := \mathbf{h}_{ri} - \mathbf{b}$, the gradient of the likelihood function

$$f(\mathbf{T},\mathbf{b}) := \sum_{i=1}^{n}\left(\frac{\|\mathbf{T}(\mathbf{h}_{ri}-\mathbf{b})\|-1}{\sigma_{mi}}\right)^2$$

is denoted by $\nabla f|_{\mathbf{x}} = [\nabla f|_{\mathbf{T}} \;\; \nabla f|_{\mathbf{b}}]$, and described by the submatrices

$$\begin{aligned} \nabla f|_{\mathbf{T}} &= \sum_{i=1}^{n}\frac{2c_T}{\sigma_{mi}^2}\mathbf{u}_i \otimes \mathbf{T}\mathbf{u}_i \\ \nabla f|_{\mathbf{b}} &= \sum_{i=1}^{n}\frac{-2c_T}{\sigma_{mi}^2}\mathbf{T}'\mathbf{T}\mathbf{u}_i \end{aligned} \tag{20}$$

where $c_T := 1 - \|\mathbf{T}\mathbf{u}_i\|^{-1}$ and $\otimes$ denotes the Kronecker product [22]. The Hessian

$$\nabla^2 f|_{\mathbf{x}} = \begin{bmatrix} \mathbf{H}_{\mathbf{T},\mathbf{T}} & \mathbf{H}_{\mathbf{T},\mathbf{b}} \\ \mathbf{H}'_{\mathbf{T},\mathbf{b}} & \mathbf{H}_{\mathbf{b},\mathbf{b}} \end{bmatrix}$$

is given by the following submatrices

$$\begin{aligned} \mathbf{H}_{\mathbf{T},\mathbf{T}} &= \sum_{i=1}^{n}\frac{2}{\sigma_{mi}^2}\left[\frac{(\mathbf{u}_i\mathbf{u}_i')\otimes(\mathbf{T}\mathbf{u}_i\mathbf{u}_i'\mathbf{T}')}{\|\mathbf{T}\mathbf{u}_i\|^3} + c_T[(\mathbf{u}_i\mathbf{u}_i')\otimes\mathbf{I}_3]\right] \\ \mathbf{H}_{\mathbf{T},\mathbf{b}} &= \sum_{i=1}^{n}\frac{-2}{\sigma_{mi}^2}\left[\frac{(\mathbf{u}_i\otimes\mathbf{T}\mathbf{u}_i)\mathbf{u}_i'\mathbf{T}'\mathbf{T}}{\|\mathbf{T}\mathbf{u}_i\|^3} + c_T(\mathbf{u}_i\otimes\mathbf{T}+\mathbf{I}_3\otimes\mathbf{T}\mathbf{u}_i)\right] \\ \mathbf{H}_{\mathbf{b},\mathbf{b}} &= \sum_{i=1}^{n}\frac{2}{\sigma_{mi}^2}\left[\frac{\mathbf{T}'\mathbf{T}\mathbf{u}_i\mathbf{u}_i'\mathbf{T}'\mathbf{T}}{\|\mathbf{T}\mathbf{u}_i\|^3} + c_T\mathbf{T}'\mathbf{T}\right]. \end{aligned} \tag{21}$$

## REFERENCES


[1] Humphreys, T. E., et al.
Magnetometer-based attitude and rate estimation for spacecraft with wire booms.
*Journal of Guidance, Control, and Dynamics*, **28**, 4 (July–Aug. 2005), 584–593.

[2] Choukroun, D., Bar-Itzhack, I. Y., and Oshman, Y.
Optimal-REQUEST algorithm for attitude determination.
*Journal of Guidance, Control, and Dynamics*, **27**, 3 (May–June 2004), 418–425.

[3] Bar-Itzhack, I. Y. and Harman, R. R.
Optimized TRIAD algorithm for attitude determination.
*Journal of Guidance, Control, and Dynamics*, **20**, 1 (1997), 208–211.

[4] Markley, F. L. and Mortari, D.
Quaternion attitude estimation using vector observations.
*The Journal of the Astronautical Sciences*, **48**, 2 (2000), 359–380.

[5] National Oceanic and Atmospheric Administration, U.S. Department of Commerce
The US/UK World Magnetic Model for 2005–2010, NOAA Technical Report, 2004.

[6] Markley, F. L.
Attitude determination and parameter estimation using vector observations: Theory.
*The Journal of the Astronautical Sciences*, **37**, 1 (Jan.–Mar. 1989), 41–58.

[7] Denne, W.
*Magnetic Compass Deviation and Correction* (3rd ed.).
Dobbs Ferry, NY: Sheridan House, 1979.

[8] Bowditch, N.
*The American Practical Navigator*.
Defense Mapping Agency, Hydrographic/Topographic Center, 1984.

[9] Gebre-Egziabher, D., et al.
Calibration of strapdown magnetometers in magnetic field domain.
*ASCE Journal of Aerospace Engineering*, **19**, 2 (Apr. 2006), 1–16.

[10] Elkaim, G. H. and Foster, C. C.
Development of the metasensor: A low-cost attitude heading reference system for use in autonomous vehicles.
In *Proceedings of the ION Global Navigation Satellite Systems Conference*, Fort Worth, TX, Sept. 2006.

[11] Alonso, R. and Shuster, M. D.
Complete linear attitude-independent magnetometer calibration.
*The Journal of the Astronautical Sciences*, **50**, 4 (Oct.–Dec. 2002), 477–490.

[12] Gambhir, B.
Determination of magnetometer biases using module RESIDG.
Computer Sciences Corporation, Technical Report 3000-32700-01TN, Mar. 1975.

[13] Crassidis, J. L., Lai, K., and Harman, R. R.
Real-time attitude-independent three-axis magnetometer calibration.
*Journal of Guidance, Control, and Dynamics*, **28**, 1 (Jan.–Feb. 2005), 115–120.

[14] Gower, J. C. and Dijksterhuis, G. B.
*Procrustes Problems* (Oxford Statistical Science Series).
New York: Oxford University Press, 2004.

[15] Foster, C. C. and Elkaim, G. H.
Extension of a two-step calibration methodology to include nonorthogonal sensor axes.
*IEEE Transactions on Aerospace and Electronic Systems*, **44**, 3 (July 2008), 1070–1078.

[16] Strang, G.
Linear Algebra and Its Applications (3rd ed.).
Florence, KY: Brooks Cole, 1988.

[17] Edelman, A., Arias, T., and Smith, S. T.
The geometry of algorithms with orthogonality constraints.
*SIAM Journal on Matrix Analysis and Applications*, **20**, 2 (1998), 303–353.

[18] Gabay, D.
Minimizing a differentiable function over a differential manifold.
*Journal of Optimization Theory and Applications*, **37**, 2 (June 1982), 177–219.

[19] Kay, S. M.
*Fundamentals of Statistical Signal Processing: Estimation*.
Upper Saddle River, NJ: Prentice-Hall, 1993.

[20] Gander, W., Golub, G. H., and Strebel, R.
Least-squares fitting of circles and ellipses.
*BIT*, **43** (1994), 558–578.

[21] Bertsekas, D. P.
*Nonlinear Programming* (2nd ed.).
Belmont, MA: Athena Scientific, 1999.

[22] Lütkepohl, H.
*Handbook of Matrices*.
New York: Wiley, 1997.

[23] Calafiore, G.
Approximation of $n$-dimensional data using spherical and ellipsoidal primitives.
*IEEE Transactions on Systems, Man and Cybernetics—Part A: Systems and Humans*, **32**, 2 (Mar. 2002), 269–278.

[24] Wahba, G.
A least square estimate of satellite attitude.
*SIAM Review*, **7**, 3 (July 1965), 409, problem 65-1.

**José Fernandes Vasconcelos** (S'06) received the Licenciatura and the Ph.D. degrees in electrical engineering from the Instituto Superior Técnico (IST), Lisbon, Portugal, in 2003 and 2010, respectively.

Since 2009, he has been a project engineer in the Advanced Projects Department at Deimos Engenharia. His research interests include nonlinear observers, inertial navigation systems, sensor calibration, and robust control with application to autonomous vehicles.

**Gabriel Hugh Elkaim** received his B.S.E. in mechanical and aerospace engineering from Princeton University, Princeton, NJ, in 1990, and his M.S. and Ph.D. from Stanford University, Stanford, CA, in aeronautics and astronautics in 1995 and 2002.

In 2003, he joined the faculty of the University of California Santa Cruz in the Computer Engineering Department, where he founded the Autonomous Systems Lab. He was promoted to Associate Professor in 2009, and his research interests are in autonomous vehicle guidance, navigation, and control, and robust sensing and estimation schemes for unmanned systems.

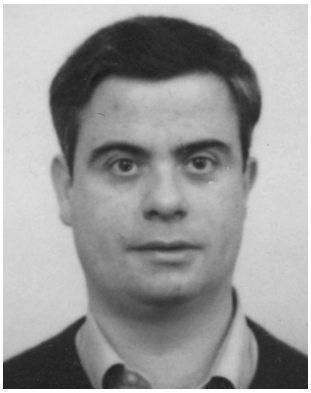

**Carlos Silvestre** (M'07) received the Licenciatura degree in electrical engineering from the Instituto Superior Técnico (IST), Lisbon, Portugal, in 1987 and the M.Sc. degree in electrical engineering and the Ph.D. degree in control science from the same school in 1991 and 2000, respectively.

Since 2000, he has been with the Department of Electrical Engineering of Instituto Superior Tecnico, where he is currently Assistant Professor of Control and Robotics. Over the past years, he has conducted research in the fields of guidance, navigation and control of single and multiple air and ocean vehicles. His research interests include linear and nonlinear control theory, coordinated control of multiple vehicles, gain scheduled control, integrated design of guidance and control systems, inertial navigation systems, and mission control and real time architectures for complex autonomous systems with applications to unmanned vehicles.

**Paulo Oliveira** (M'92) received the Ph.D. degree in 2002 from the Instituto Superior Técnico (IST), Lisbon, Portugal.

He is currently an assistant professor in the Department of Electrical and Computer Engineering at IST. He is a researcher in the Institute for Systems and Robotics Associate Laboratory, Lisbon, and his current research interests include robotics and autonomous vehicles with special focus on the fields of nonlinear estimation, sensor fusion, navigation, positioning, and advanced signal processing techniques.

Dr. Oliveira has participated in fifteen Portuguese and European research projects and is the author of more than one hundred conference and journal papers.

**Bruno Cardeira** received the Licenciatura and the M.Sc. degrees in electrical engineering from the Instituto Superior Técnico (IST), Lisbon, Portugal, in 2003 and 2009, respectively.

He is currently with the Dynamical Systems and Ocean Robotics (DSOR) Laboratory, at the Institute for Systems and Robotics (ISR), IST.